



HAL
open science

Decadal beach-dune profile monitoring along a 230-km high-energy sandy coast: Aquitaine, southwest France

A. Nicolae Lerma, B. Castelle, V. Marieu, A. Robinet, T. Bulteau, N. Bernon, C. Mallet

► To cite this version:

A. Nicolae Lerma, B. Castelle, V. Marieu, A. Robinet, T. Bulteau, et al.. Decadal beach-dune profile monitoring along a 230-km high-energy sandy coast: Aquitaine, southwest France. *Applied Geography*, 2022, 139, pp.102645. 10.1016/j.apgeog.2022.102645 . hal-03831762

HAL Id: hal-03831762

<https://hal.science/hal-03831762>

Submitted on 27 Oct 2022

HAL is a multi-disciplinary open access archive for the deposit and dissemination of scientific research documents, whether they are published or not. The documents may come from teaching and research institutions in France or abroad, or from public or private research centers.

L'archive ouverte pluridisciplinaire **HAL**, est destinée au dépôt et à la diffusion de documents scientifiques de niveau recherche, publiés ou non, émanant des établissements d'enseignement et de recherche français ou étrangers, des laboratoires publics ou privés.

1 **Decadal beach-dune profile monitoring along a 230-km high-energy mesotidal sandy coast**

2 A. Nicolae Lerma^{1,2}, B. Castelle^{3,4}, V. Marieu^{3,4}, A. Robinet^{1,2}, T. Bulteau^{1,2}, N. Bernon^{1,2}, C. Mallet^{1,2}

3 Draft article for *Applied Geography*

4 ¹BRGM French Geological Survey, Regional Direction Nouvelle- Aquitaine, Pessac, France

5 ² Observatoire de la Côte Aquitaine (OCA), Pessac, France

6 ³CNRS, UMR 5805 EPOC, Pessac, France

7 ⁴Université de Bordeaux, UMR 5805 EPOC, Pessac, France

8

9

10 **Highlights:**

- 11 • Analysis of a 11-year beach profile dataset along 230 km of high-energy sandy coast
- 12 • All morphological descriptors are characterized by a north-south gradient
- 13 • Timing and magnitude of beach-dune recovery from the 2013-14 winter is variable
- 14 • Shoreline change trends range from -5.9 m/year to +2.1 m/year
- 15 • Post-winter beach-dune volume is a good proxy of shoreline change trend

16

17 **Keywords:** beach profile; erosion; recovery; regional variability; coastal dune; long-term trend

18

19

20

21

22

23

24

1 Decadal beach-dune profile monitoring along a 230-km high-energy mesotidal sandy coast

2

3 **Abstract:**

4 Large-scale coastal monitoring programs are challenging to maintain in time but are necessary to
5 understand and further predict complex coastal evolution and resilience. The 230-km-long Aquitaine
6 coast is a high-energy meso-macrotidal coast composed of beach-dune systems showing dramatic
7 morphological changes at seasonal and interannual scales. This study investigates the alongshore
8 variability in beach-dune response based on a unique 11-year dataset of 41 adequately spaced
9 transects surveyed yearly in spring. The dataset is completed by interspersed autumn LiDAR surveys
10 for seasonal analysis. Several beach-dune morphological descriptors are developed, such as beach-
11 dune volume, beach width and different shoreline proxies delimiting the intertidal zone, the beach
12 face and the dune face. The Aquitaine beach-dune system is characterised by a north-south gradient,
13 from chronically eroding dunes backing low-elevation dissipative beaches in the north, to slowly
14 accreting dunes backing wide and healthy beaches in the south, through a range of intermediate
15 beach-dune states. Time- and spatially-averaged shoreline (dune foot position) trend is -0.5 m/year
16 (erosion), with local variations ranging from -5.9 m/year to +2.1 m/year. During the 2013-2014 winter
17 widespread erosion was observed, with the shoreline eroding by 13 m and 8 m on average along the
18 Gironde and Landes coasts, respectively. This dataset provides insight into the timing, magnitude and
19 spatial variability of beach-dune recovery from the outstandingly erosive 2013-2014 winter. We also
20 show that local beach-dune volume is a good proxy for long-term shoreline trend. It is advocated that
21 such large-scale coastal monitoring by means of single beach profiles adequately spaced and
22 distributed along 10-100 kilometres of coast is a cheap and efficient approach to address coastal
23 changes at regional scale, which can bring complementary information to aerial photographs
24 interpretation to determine long-term shoreline evolution trend and thus contribute to support
25 sustainable coastal management and planning.

26
27
28
29
30
31
32
33
34
35
36
37
38
39
40
41
42
43
44
45
46
47
48
49
50
51
52
53

1. Introduction

Sandy coasts are attractive environments that are increasingly threatened by climate change combined with other factors such as natural shortage of sediment supply and human activities interfering with natural processes. Coastal management and planning require improved understanding of past shoreline evolution and its drivers. Coastal changes along sandy coasts cover a wide range of time scales, from hours (storms) to chronic, through large seasonal and interannual variability (Stive, 2004). This time variability is reflected in the evolution of the shoreline position for most existing proxies (Boak and Turner, 2005), and in the detailed evolution of the beach-dune profile. Storm-driven beach and dune erosion typically occurs over hours to days (e.g. Harley et al., 2017), but beach recovery typically takes days to months (Phillips et al., 2019; Castelle and Harley, 2020), while foredune recovery can take years to decades (e.g. Morton et al., 1994; Lee et al., 1998). Different erosion/recovery stages can therefore be observed along the beach-dune profile, e.g. with a wide (accreted) beach backed by a scarped (eroded) dune. Such complex beach-dune profile behaviours, which are critical to

54 understand and further predict the system resilience, can only be addressed through dedicated long-
55 term (decades) monitoring programs.

56 Natural spatial variability of sandy coasts can be large, with stable, eroding, and accreting sectors
57 typically alternating on the regional scale (kilometres to 10s of kilometres, e.g. [Ruggiero et al., 2005](#),
58 [Héquette et al., 2019](#)). Beach state and dominant temporal modes of variability can also strongly vary
59 at this spatial scale ([Short and Wright, 1983](#)). Different factors can control this variability, such as the
60 presence of tidal inlet or estuary mouth ([Castelle et al., 2018](#); [Chaumillon et al., 2019](#); [Konlechner et](#)
61 [al. 2020](#)), sediment supply from the shoreface ([Anthony, 2013](#)), coastal structures or natural headlands
62 disrupting longshore sand transport ([Anderson et al., 2018](#)), or variable exposure to storm waves ([Scott](#)
63 [et al., 2011](#)).

64 Large-scale coastal monitoring programs are nowadays typically based on LiDAR surveys (e.g. [Sallenger](#)
65 [et al., 2003](#), [Saye et al., 2005](#); [Houser et al., 2008, 2015](#), [Pye and Blott 2016](#), [Burvingt et al., 2017](#); [Le](#)
66 [Mauff et al., 2018](#); [Nicolae Lerma et al., 2019](#)). However, LiDAR surveys are costly and difficult to
67 maintain on the long-term on a yearly basis. They have been implemented only recently, therefore
68 currently limiting the length of available time series. In contrast, publicly available satellite imagery can
69 provide large-scale data from local to global scale for free (e.g. [Vos et al., 2019](#)). However, the inferred
70 data is restricted to shoreline position, with decreased accuracy in meso- and macro-tidal high-energy
71 environments ([Castelle et al., 2021](#)). Instead, since the 90-2000s GNSS tools have been widely used as
72 a flexible and accurate approach to survey beach morphology change over the time ([Morton et al.,](#)
73 [1993](#); [Larson and Kraus 1994](#)). GNSS tools therefore dramatically increased the number of beach
74 monitoring programs worldwide, which were scarce before the 80's (see [Harley et al., 2011](#) for a
75 review). Over the years, such monitoring programs progressively provided insight into seasonal and
76 interannual beach variability, including response and recovery from severe storms (amongst others,
77 [Ruiz de Alegria-Azuburu and Masselink, 2010](#) ; [Ranasignhe et al., 2011](#) ; [Harley et al., 2011](#), [Barnard et](#)
78 [al., 2012](#) ; [Suanez et al., 2012](#) ; [Masselink et al., 2014](#) ; [Bracs et al., 2016](#) ; [Scott et al., 2016](#) ; [Castelle et](#)
79 [al., 2020](#)). However due to practical reasons, such GNSS coastal monitoring programs are generally

80 dedicated to a single site, covering no more than a few kilometres and/or focusing on the beach system
81 and thus disregarding the backing dune (Stokes et al., 2015). At regional scale, say 10s to 100s of
82 kilometres, long term GNSS beach survey programs made of profiles spaced at 100s to 1000s of meters
83 are scarce (Ruggiero et al., 2005, Short et al., 2014, Chaumillon et al., 2019) and are limited to coastal
84 environments with prominent geological setting and a wide range of wave exposure. Such settings
85 result in contrasting and dichotomic morphological and response types that can be further clustered
86 (Bunningham and French, 2017; Konstantinou et al 2021). A notable exception is the beach monitoring
87 program developed along the high-energy coasts of northwest Oregon and southwest Washington,
88 USA (Ruggiero and Voigt, 2000, Ruggiero et al., 2005). This stretch of coast is approximately exposed
89 to the same wave climate, with a complex variability in nearshore system morphology and response
90 type (Ruggiero et al., 2005), challenging morphological and response type classification. To the best of
91 the authors' knowledge there is no equivalent beach monitoring program elsewhere.

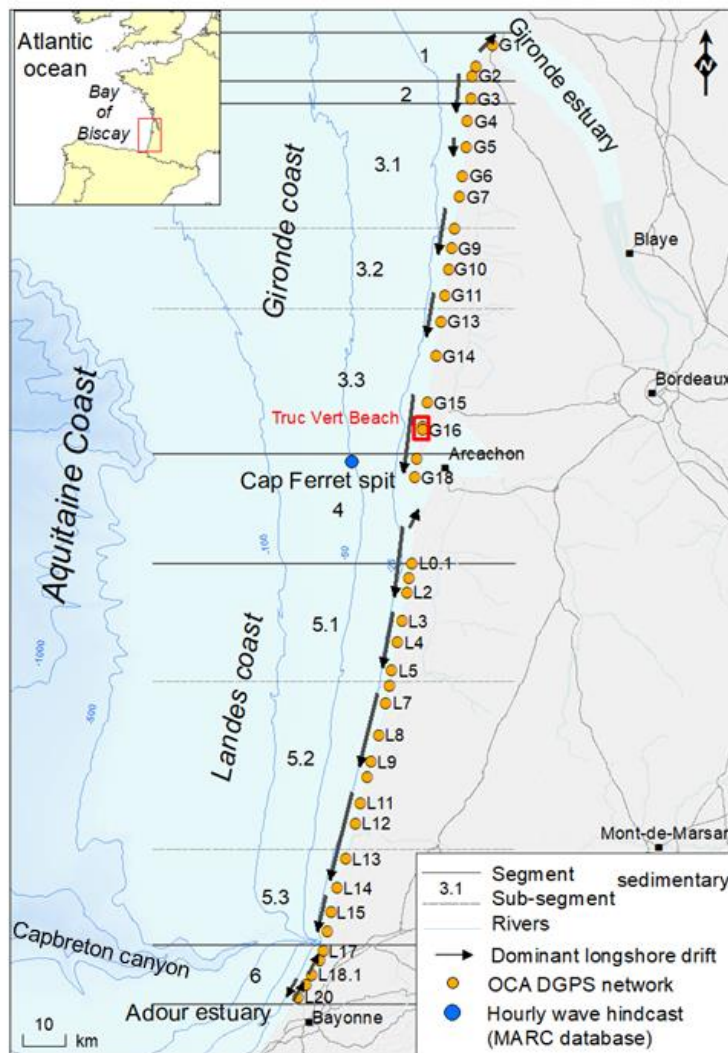
92 In this paper, we present a new 11-year regional monitoring dataset starting in 2008, made of 41
93 beach-dune profiles distributed along the c. 230-km high-energy meso- to macro-tidal Aquitaine coast,
94 southwest France. Several morphological descriptors are computed and combined to address
95 shoreline evolution and coastal change at regional scale, including the variability of responses and
96 multi-year recovery from the outstanding 2013-2014 winter. These results are compared with other
97 approaches used to determine long-term shoreline evolution trends and implication of past trend
98 extrapolation are discussed.

99

100 **2. Study area**

101 The sandy coast of Aquitaine extends approximately 230 km from the Gironde estuary in the north to
102 the Adour Estuary in the south. It can be further divided into two large sectors, the Gironde and the
103 Landes coasts separated by the Arcachon Lagoon inlet (Figure 1). While the coast is exposed to the

104 same wave climate and is seemingly uniform, the coastal system shows substantial morphological
 105 alongshore variability.



106
 107 Figure 1: Location map of the study area with indication of the coastal segments and sub-segments,
 108 net longshore drift intensity and direction, beach transect locations and wave hindcast grid point (Cap
 109 Ferret buoy).

110 2.1. Wave and tide conditions

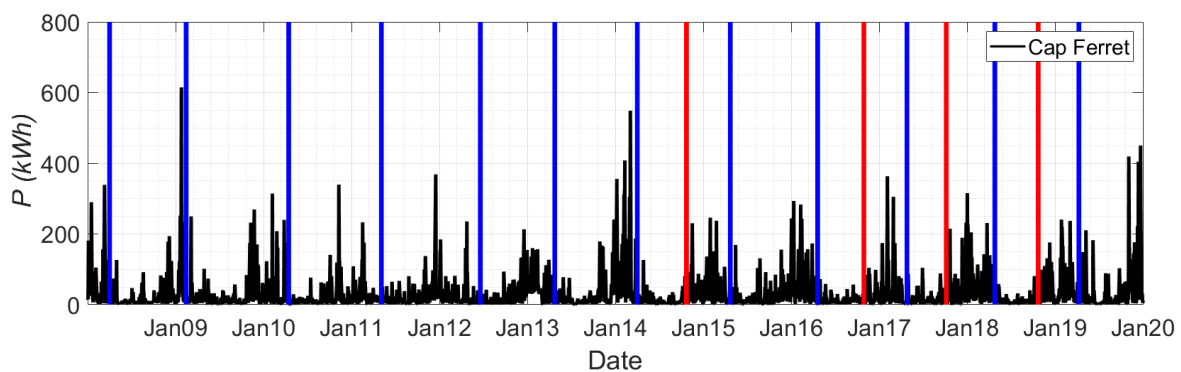
111 The tide regime and wave climate are relatively homogeneous along the Aquitaine coast. It is a meso-
 112 to macrotidal environment, with an annual mean tidal range of c. 3.7 m and a maximum tidal range
 113 reaching 5 m during spring tides, with slightly lower tide range in the south. On the open coast, storm
 114 surge (non-tidal residual) is small (< 1 m).

115 The wave climate is energetic and strongly seasonally modulated with a monthly-averaged significant
 116 wave height H_s (peak wave period T_p), ranging from 1.1 m (8.5 s) in July with a dominant west-
 117 northwest direction, to 2.4 m (13 s) in January with a dominant west direction (Castelle et al., 2017a).
 118 Winter-mean wave activity shows large interannual variability enforced by large-scale climate patterns
 119 of atmospheric variability, primarily the West Europe Pressure Anomaly (WEPA) and to a lesser extent
 120 the North Atlantic Oscillation (NAO) (Castelle et al., 2017b). The modal wave direction is from the west-
 121 northwest and from the northwest in the northern and southern part of the coast, respectively.
 122 Extreme wave conditions also show a slight latitudinal gradient, with the 100-year return H_s varying
 123 from 11 m in the north to 11.6 m in the south (Nicolae Lerma et al., 2015).

124 Figure 2 shows the 2008-2020 time series of the wave energy flux, P (kW/m), calculated in deep water
 125 according to the following equation (Tucker and Pitt 2001):

$$P = \frac{\rho g^2}{64\pi} T_p H_s^2$$

126
 127 where ρ is the density of sea water (1030 kg/m³), g the gravitational acceleration (9.81 m/s²), with H_s
 128 and T_p extracted at the Cap Ferret buoy (in c. 50 m depth at 1.447°W; 44.653°N, see Figure 1) from
 129 MARC platform (Modelling and Analysis for Research in Coastal environment, www.umr-
 130 lops.org/marc)



131
 132 Figure 2: Time series of computed wave energy flux (P) at Cap Ferret buoy grid point (Figure 1) over
 133 the period 2008-2019. Vertical lines indicate the occurrence of topographic surveys by GNSS (blue) and
 134 LiDAR (red).

135 **2.2. Longshore drift and beach-dune morphology**

136 The prevailing west-northwest wave direction drives a net southerly longshore drift along most of the
137 coast, except at the northern and southern end of the coast where the longshore drift reverses as a
138 result of a change in coastal orientation (Figure 1). According to Idier et al. (2013) the mean residual
139 longshore drift increases southwards from c. $200 \cdot 10^3$ to $400 \cdot 10^3$ m³/yr along most of the Gironde coast.
140 The residual longshore drift along the Landes coast decreases progressively southwards from c.
141 $700 \cdot 10^3$ to $500 \cdot 10^3$ m³/yr before dramatically dropping near the Capbreton Canyon.

142 Beaches are intermediate double barred. The inner intertidal bar shows most of the time a transverse
143 bar and rip morphology. In contrast, the outer subtidal bar is modally crescentic. Overall, both inner
144 and outer bar rip spacing increases southwards (Lafon et al., 2002; BRGM and ONF, 2018), with the
145 outer bar wavelength sometimes exceeding 1000 m. These sandbars act as an efficient protection of
146 the beach/dune system as they dissipate storm wave energy offshore through depth-induced breaking.
147 Erosive megacusps cutting the dune during severe storm events can also be enforced by the outer bar
148 morphology through large-scale rips, further exposing the dune to wave attack (Castelle et al., 2015).

149 The subaerial beach-dune profile typically exhibits a berm after periods of fair weather conditions,
150 sometimes with superimposed beach cusps. Such beach berm dynamics is less pronounced in the north
151 of the study area, whereas beaches in the south are steeper and can exhibit superimposed generations
152 of berms. The beach-dune system also shows incipient foredune and foredune scarps alternating in
153 both time (Castelle et al., 2017a) and space (Nicolae Lerma et al., 2019). Since the outstanding 2013-
154 2014 winter (Figure 2) that eroded the dune along almost the entire coast, most of the beach-dune
155 system has been slowly recovering and currently shows incipient foredunes at different stages of
156 maturity (Nicolae Lerma et al., 2019).

157 **2.3. Alongshore segmentation of the coast**

158 The coast has previously been subdivided into relatively homogeneous segments or sub-segments
159 (BRGM and ONF, 2018, Nicolae Lerma et al., 2019) based on the (i) variability in direction and intensity

160 of the dominant longshore drift (Idier et al., 2013), (ii) nearshore sandbar configuration (Lafon et al.,
161 2002), (iii) seasonal beach slope variability (Bulteau et al., 2016), (iv) sediment grain size (Pedreros,
162 2000), (v) dune morphology and dynamics (Bossard and Nicolae Lerma 2020). The resulting six
163 segments, subdivided into three sub-segments for the central part of the Gironde and Landes coasts
164 are shown in Figure 1. They are used hereafter to investigate the alongshore-variable beach-dune
165 evolutions over a decade, including the assessment of timing and magnitude of beach-dune recovery
166 from the 2013-2014 winter.

167

168 **3. Material and methods**

169 **3.1. GNSS Topographic data**

170 Since April 2008, the beach-dune morphology has been surveyed along the entire Aquitaine coast after
171 each winter by the Observatoire de la Côte Aquitaine (OCA). Surveys are performed by foot at low tide
172 with a centimetric GNSS, from the water line to the back of the dune. The beach-dune profiles are
173 collected at 55 transects distributed along the Aquitaine coast. In the present study we focus on open
174 natural beaches, therefore seven transects located at coastal resorts or in the alignment of busy beach
175 access and five transects adjacent to small river mouths or within the Arcachon lagoon were
176 disregarded. Two transects with more than 2 years of missing data were also disregarded, resulting in
177 a dataset of 41 post-winter profiles from 2008 to 2019, with 19 located in Gironde and 22 in Landes
178 (Figure 1).

179

180 **3.2. LiDAR Data**

181 Several airborne LiDAR campaigns from the OCA database acquired in collaboration with the French
182 National Institute of Geography (IGN) were used. Data were acquired during fall 2014, and annually at
183 the same period since 2016. LiDAR Digital Terrain Models (DTMs) were systematically checked with

184 over a thousand of salient fixed ground control points showing vertical errors under 0.15 m (Nicolae
185 Lerma et al., 2019). A summary of the LiDAR data characteristics and associated errors is presented in
186 Table 1. LiDAR data was extracted along the 41 survey transects described in Section 2.2.1, providing
187 pre-winter beach-dune profiles (2014, 2016, 2017, 2018), thus completing the post-winter GNSS
188 dataset.

189 Table 1: Acquisition dates and altimetric errors of LiDAR campaigns

LiDAR survey campaign	Acquisition date	Altimetric error Z (m)
2014	October 23 – 24	0.144
2016	October 29 – 30	0.106
2017	October 4 - 6 and 7	0.102
2018	October 23 – 24	0.096

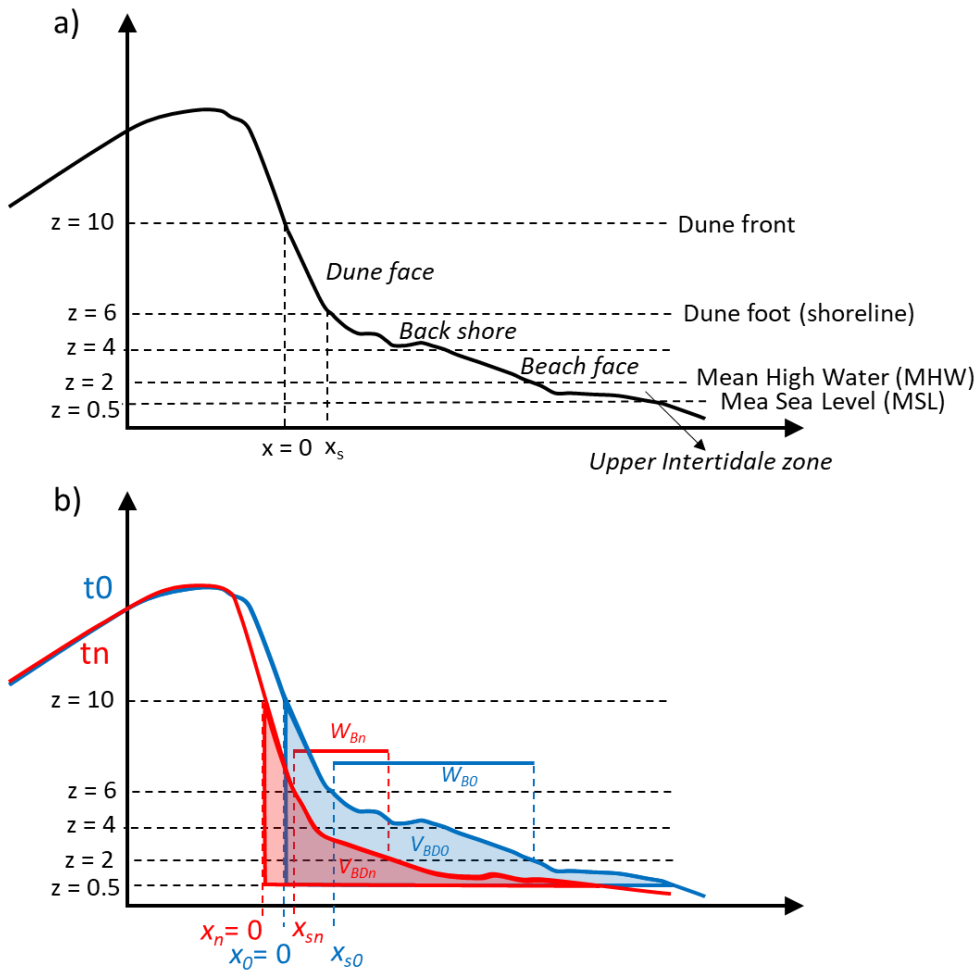
190

191 3.3. Beach-dune profile analysis

192 Four vertical elevations were used to discriminate different profile sections and to further compute
193 shoreline and beach volume proxies (Figure 3a). In line with previous works (Bulteau et al., 2016;
194 Castelle et al., 2017a, Biauxque et al., 2019, Nicolae Lerma et al., 2019), the upper limit of the intertidal
195 zone was defined as $z = 2$ m NGF (official levelling network in mainland France), which is approximately
196 the Mean High Water (MHW) elevation along the coast (SHOM 2016), while the upper limit of the
197 beach was defined as $z = 4$ m NGF under which seasonal beach variation and berm dynamics is
198 observed. The shoreline, $z = 6$ m NGF, roughly corresponds to the time and space average dune foot
199 elevation along the coast (Nicolae Lerma et al., 2019). This elevation was used to discriminate the
200 beach from the dune compartment and to further compute the shoreline position (x_s). Of note, the
201 dune foot elevation varies along the Aquitaine coast, between less than 5 m NGF in the north (Seg 1
202 and 2) and more than 7 m NGF in the south (Seg 6). The dune foot height at a given location may also

203 vary seasonally, with wave attack lowering the dune foot, and under constructive onshore winds rising
204 it. However, the assumption of a constant value of 6 m NGF is reasonable for conducting a regional-
205 scale decadal analysis of beach-dune profiles. Finally, $z = 10$ m NGF was used to identify the landward
206 limit of the dune face up to where wave-driven erosion during severe storms and slow wind-driven
207 recovery can be depicted. Of note, the dune elevation can exceed 20 m in some locations (Bossard and
208 Nicolae Lerma 2020), however the 10 m level was preferred to allow following and further comparing
209 the entire range of dune profiles observed along the coast. Two beach-dune descriptors were
210 subsequently derived: (i) the beach width (W_B), defined as the horizontal distance between the profile
211 intersections with the 2 m and 6 m NGF elevations ; (ii) the beach-dune volume (V_{BD}), defined as the
212 sediment volume between the profile intersections with the mean sea level (0.5 m NGF) and 10 m NGF
213 computed in m^3/m . Interannual and seasonal V_{BD} changes defined as the differences in absolute value
214 between two successive annual surveys and between two successive seasonal surveys, respectively,
215 were also computed. These four vertical datum allowed defining four distinct compartments: (i) The
216 upper intertidal zone between (0.5-2 m NGF); (ii) the beach face between (2-4 m NGF); (iii) the back
217 shore (4-6 m NGF); (iv) the dune face compartment between 6 m NGF and 10 m NGF.

218 The variability in beach-dune profile shape along the coast was also analysed. Given the large changes
219 in both time and space of the beach-dune profiles, a local reference frame was used. For each beach-
220 dune profile collected, the data was translated so that local cross-shore position $x = 0$ systematically
221 corresponds to the intersection of the beach-dune profile with the 10 m NGF datum (Figure 3B). For
222 each transect, beach-profile envelope and mean profiles were further computed. This local reference
223 frame was preferred to compare beach-profile shapes and envelopes.



224

225 Figure 3: Schematics of the beach-dune profile analysis at a given transect: a) beach-dune profile
 226 compartments b) shoreline position (x_s) and morphological descriptors: beach width (W_B) between $z =$
 227 2 m and $z = 6$ m, and beach-dune volume (V_{BD}) between $z = 0.5$ m and $z = 10$ m. In order to compare
 228 beach-dune profile shape in both time and space (see Figure 4) a local reference frame is used in which
 229 for each profile $x = 0$ is defined as the intersection of the beach-dune profile with elevation $z = 10$ m.

230

231 4. Results

232 4.1. Spatio-temporal variability of the beach dune morphology

233 Figure 4 shows the superimposed beach-dune profiles for each segment and sector, as well as their
 234 temporal mean and pre-/post-winter profile envelopes in local reference frame. The statistics of beach

235 width (W_B), beach-dune volume (V_{BD}) for all profiles discriminated as pre- and post-winter are provided
236 in [Table 2](#). Results show dramatic changes of beach-dune profile characteristics in both time and space.
237 Seg 1 and 2 in the north of the study area show the less variable beach-dune profile shapes, with a
238 mostly flat to slightly concave foreshore domain, and a steep face above c. 4 m NGF (dune scarping).
239 The average W_B at these sectors is narrow (32-40 m) with a maximum amplitude around the mean of
240 only 31 m. This reasonably small time and spatial variability is also reflected in the profile elevation
241 variability and, in turn, in V_{BD} variability ([Table 2](#)). At the other end of the spectrum, beach-dune
242 profiles at the southern end of the study area (Seg 6) show much wider and more variable
243 morphologies, sometimes displaying convex shape typical of accreting bermed beaches. For instance
244 at Seg 6, V_{BD} (W_B) varies between 132 and 745 m³/m (35 and 82 m), with envelope vertical amplitude
245 exceeding 8 m where berm dynamics is observed ([Figure 4](#)). Between these two end members, beach-
246 dune profiles show intermediate characteristics. Some transects can locally show different
247 characteristics ([Figure 5](#)), e.g. immediately updrift of the Arcachon tidal inlet (transect G18) or updrift
248 of the Adour training wall (transect L20), suggesting some tidal and anthropogenic influence on the
249 profile dynamics, respectively. Overall, beach-dune profiles along the Gironde and Landes coasts are
250 characterized by a north-south gradient in all descriptors ([Figure 5](#)), indicating progressively wider
251 beaches, thicker envelopes, and larger V_{BD} southwards.

Table 2: Statistics of beach-dune profile descriptors for all segments and sectors

Segment	Effectif	W_B (m)			Post-winter	Pre-winter	V_{BD} (m ³ /m)			Post-winter	Pre-winter	Interannual	Seasonal
		mean	min	max	W_B (m)	W_B (m)	mean	min	max	V_{BD} (m ³ /m)	V_{BD} (m ³ /m)	V_{BD} difference (m ³ /m)	V_{BD} difference (m ³ /m)
Seg1	3	32	23	45	32	33	151	81	308	157	168	24	31
Seg2	1	40	26	57	36	50	232	116	269	173	242	20	38
Seg3	13	51	29	90	45	66	278	106	594	261	327	50	74
Seg4	2	58	31	99	53	71	395	132	758	379	438	72	100
Seg5	17	61	35	90	57	69	327	157	603	314	360	52	57
Seg6	5	59	35	82	58	62	410	132	745	398	443	43	34
Gironde	19	49	23	99	45	63	266	81	758	251	308	46	68
Landes	22	59	35	90	57	66	345	132	745	333	379	50	52
Totale	41	55	23	99	51	65	308	81	758	295	347	48	58

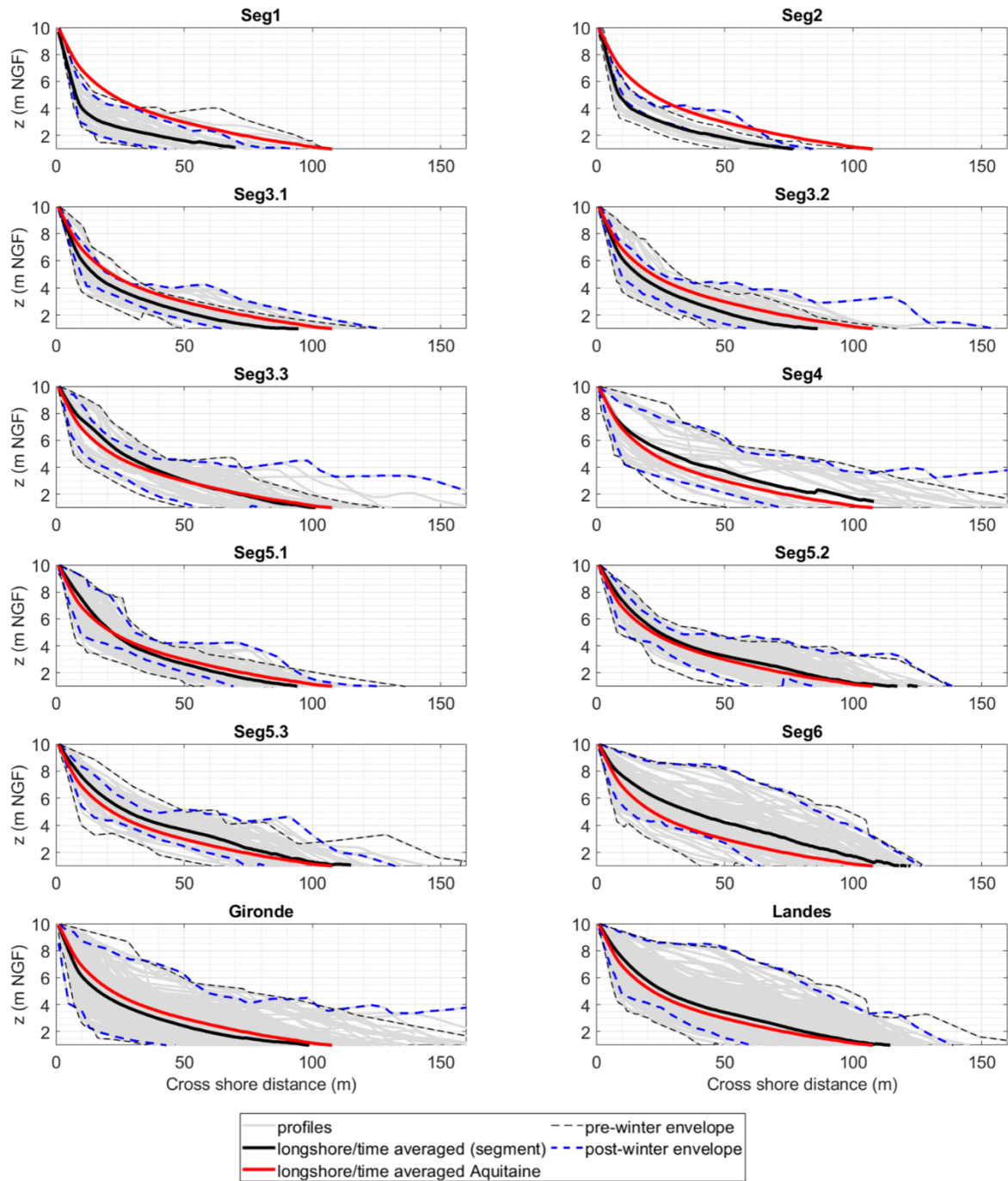


Figure 4: Pre/post-winter profiles and statistical values, gathered by segment and sector (Gironde and Landes). Spatially- (Gironde and Landes) and time-averaged pre/post-winter profiles are superimposed (black curve) for each segment and sector (Gironde and Landes). The red profile in all panels is the Aquitaine-averaged. Envelopes of post-winter and pre-winter profiles are represented by the black and blue dashed curves, respectively.

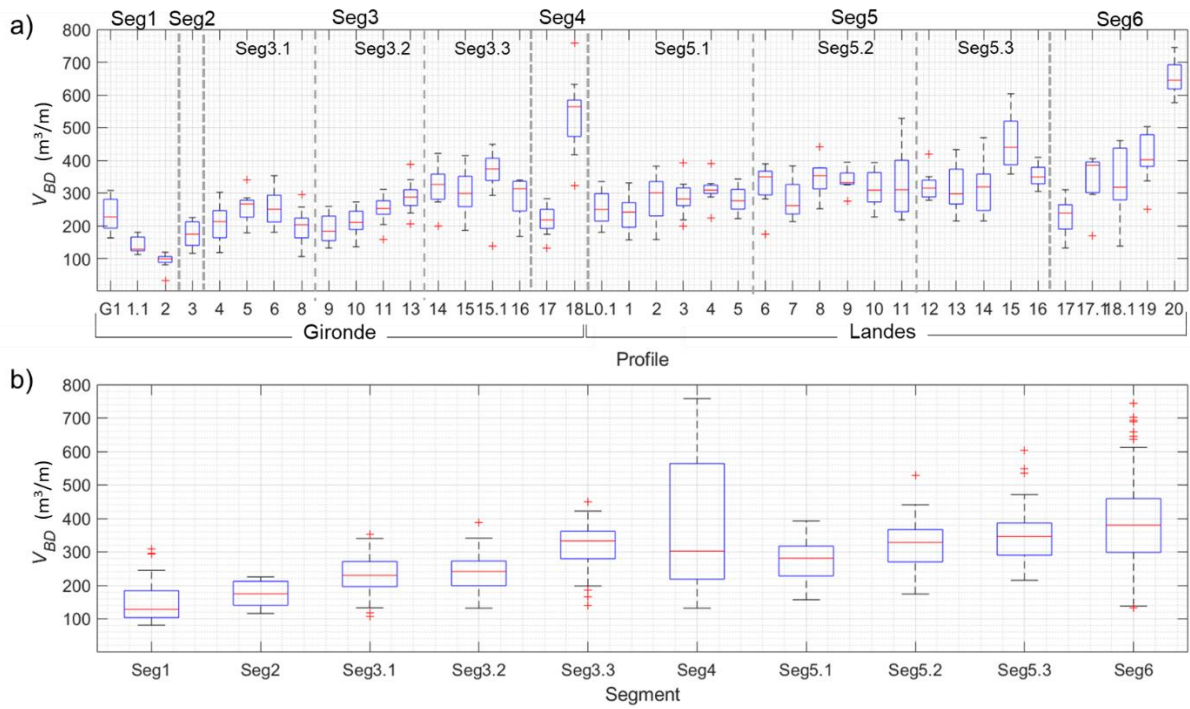


Figure 5: Box plot of beach-dune volume V_{BD} (period 2008-2019) for (a) all transects along the Gironde and Landes coasts, and (b) averaged by coastal segment. The central horizontal marks in the box plots indicate the median, and the top and bottom edges of the blue boxes indicate the 25th and 75th percentiles, respectively. Maximum whisker length extends up to 1.5 times the interquartile range and the outliers are plotted individually using the '+' symbol.

4.2. Temporal variability

Figure 6 (left-hand panels) shows the 2008-2019 time series of post-winter W_B , V_{BD} and x_s for the Gironde and Landes sectors, further zooming onto the 2014-2019 period combining the pre- and post-winter profiles using LiDAR data. An increasing trend in both W_B (+13%) and V_{BD} (+15.1%) is observed (Figure 6a,b), despite x_s severely retreated during the 2013-2014 winter (Figure 6c). Sector-averaged interannual and seasonal W_B and V_{BD} absolute differences were computed (Table 2). On average along the entire coast, pre-winter V_{BD} is larger than post-winter V_{BD} by 58 m^3/m . However, notable differences are observed between the Gironde and Landes coasts, with pre-post-winter V_{BD} differences

of $68 \text{ m}^3/\text{m}$ and $52 \text{ m}^3/\text{m}$ in Gironde and Landes, respectively. Landes and Gironde interannual V_{BD} differences are more subtle, i.e. of 50 and $46 \text{ m}^3/\text{m}$, respectively (Table 2).

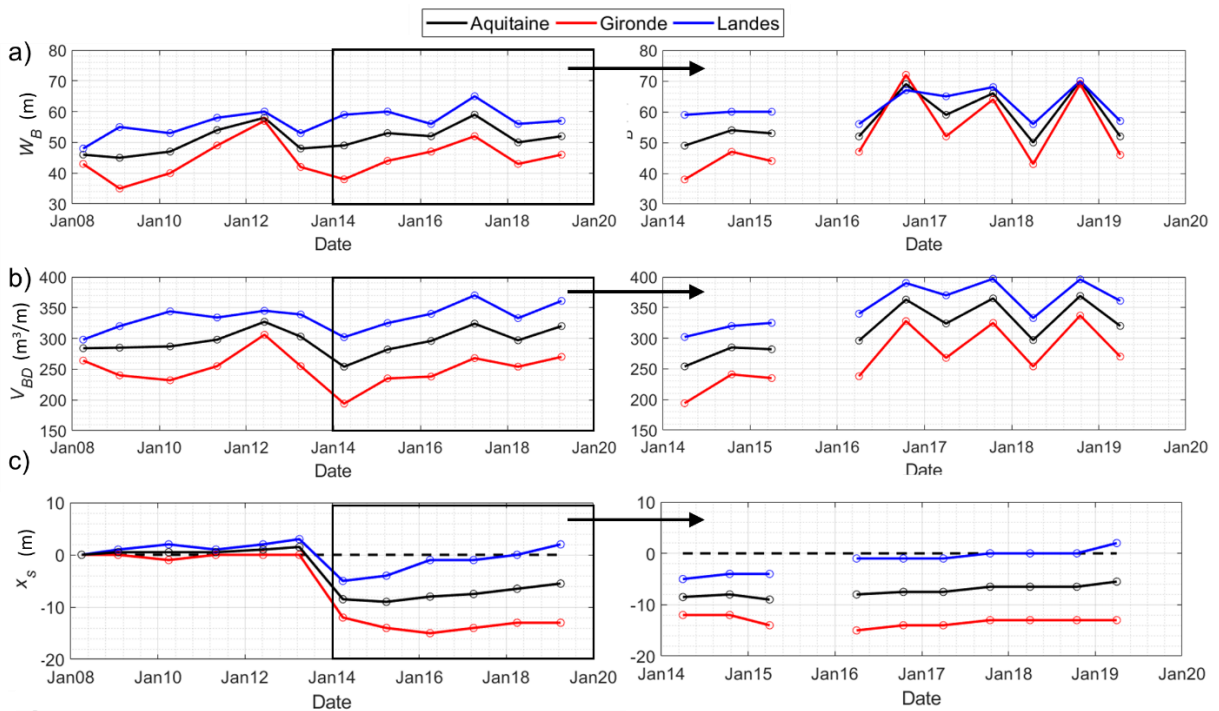


Figure 6: Post-winter (2008-2019, left-hand panels) and pre/post-winter (2014-2019, right-hand panels) (a) beach width W_B , (b) beach-dune volume V_{BD} and (c) shoreline position x_s (6 m NGF) relative to 2008 shoreline position, averaged along the Gironde coast (red), Landes coast (blue) and along the entire coast (black).

Figure 7 shows the 2008-2019 time series of the intersection between the profile and different elevations, averaged for the Landes and Gironde sectors. The lower part of the profile (2-m and 4-m elevation positions which delimitate the beach face) systematically show the largest variability on both seasonal (right-hand panels) and interannual (left-hand panels) timescales. The 6-m and 10-m elevation positions, which correspond to the dune foot and our definition of the upper limit of the dune face, respectively, show more stable position in time, except during the 2013-2014 winter that caused the elevation positions to retreat by 13 m and 8 m (8 m and 3 m), respectively, for the Gironde (Landes) coast. The 2013-2014 winter impact was clearly more pronounced along the Gironde coast than along the Landes coast, especially near the higher part of the profiles as dune erosion in Landes was limited.

In addition, while the 6-m (x_s) and 10-m elevation positions in the Landes sector show slow but full recovery from that outstanding winter, erosion continued in Gironde, which is primarily the signature of the chronic erosion occurring in the northern part of the coast (Seg 1, 2, 3.1 and 3.2, Figure 10).

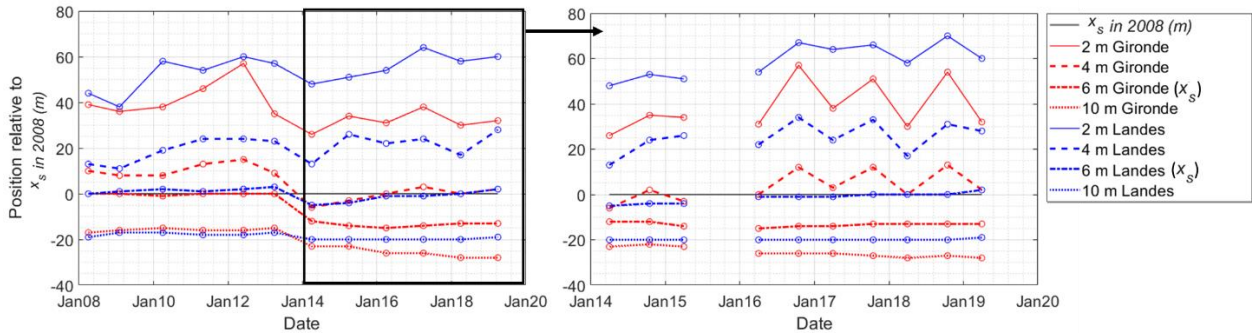


Figure 7: Time series of 2008-2019 post-winter (left-hand panel) and 2014-2019 pre/post-winter (right-hand panel) cross-shore position of different beach elevation proxies: upper limit of the intertidal zone ($z = 2$ m NGF), the upper beach limit ($z = 4$ m NGF), dune foot x_s ($z = 6$ m NGF) and our definition of the upper limit of the dune face ($z = 10$ m NGF), averaged over Gironde and Landes coasts.

3.3 Shoreline evolution trend and beach-dune volume

Figure 8 shows the spatial distribution of average shoreline change rate against beach-dune volume. On average, x_s retreated by c. 5.4 m (0.5 m/yr), with large alongshore variability. In brief, the average retreat is 14 m (1.2 m/yr) in Gironde and is only 0.9 m (0.1 m/yr) in Landes. More locally, the most severe retreats are observed within Seg 1, at transects G1.1 and G2 with 44 m (4 m/yr) and 65 m (5.9 m/yr), respectively. Accreting sectors over the 2008-2019 period are scarce and are essentially located along the Landes coast at Seg 5.2 and 6, with maximum accretion of 10 m (0.9 m/yr) and 23 m (2.1 m/yr). Shoreline evolution change rate (x_s/dt) is well correlated to the time-averaged beach-dune volume V_{BD} following a log relation both using post-winter ($r^2 = 0.75$), and pre-winter ($r^2 = 0.69$) V_{BD} (Figure 8), indicating that shoreline erosion rate increases with decreasing beach-dune volume V_{BD} . For instance, Seg1 and Seg2 located in the rapidly eroding Gironde coast are characterized by post-winter

V_{BD} lower than $150 \text{ m}^3/\text{m}$ ($200 \text{ m}^3/\text{m}$ in pre-winter situation). Conversely, beaches with a post-winter V_{BD} larger than $360 \text{ m}^3/\text{m}$ are scarce but systematically stable or significantly accreting ($> 1 \text{ m}/\text{year}$). Post-winter V_{BD} between 280 and $360 \text{ m}^3/\text{m}$ characterize beaches presenting relatively stable x_s (between $\pm 1 \text{ m}/\text{year}$) over the period 2008 and 2019. No stable or accreting beach profile are observed for post-winter V_{BD} under $280 \text{ m}^3/\text{m}$. This suggests that the time-average V_{BD} , here post-winter, is a good proxy for long-term shoreline change trends along this coast. Beaches with V_{BD} higher than $280 \text{ m}^3/\text{m}$ can recover from an outstanding winter within a few year and, on the contrary, beaches with V_{BD} lower than $280 \text{ m}^3/\text{m}$ are chronically eroding.

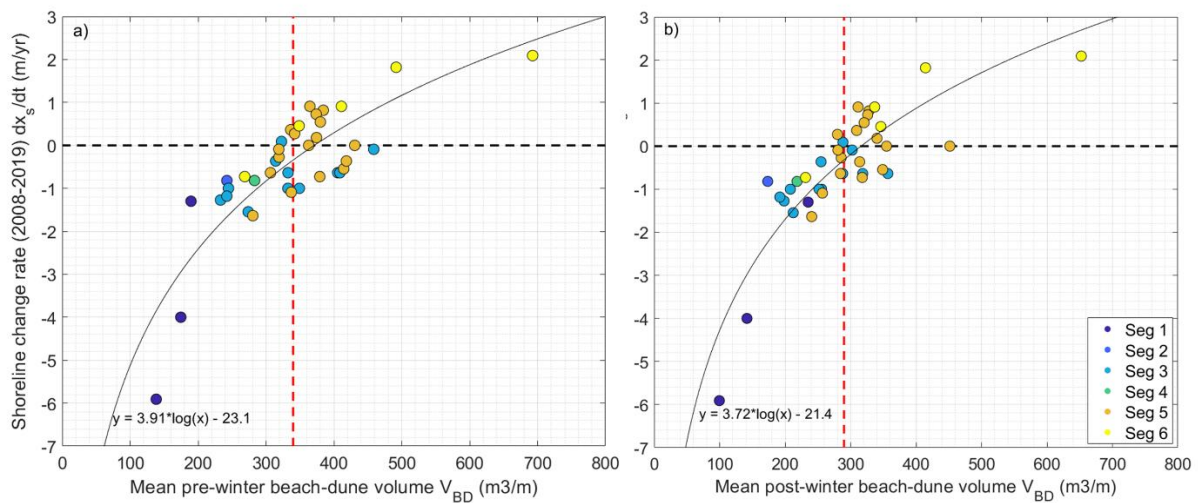


Figure 8: Average shoreline change rate (dx_s/dt) over 2008-2019 against (a) mean pre-winter beach-dune volume (V_{BD}) and against (b) mean post-winter beach-dune volume (V_{BD}). The solid black line is the log regression curve. The vertical dashed red line is the time and spatially averaged beach-dune volume.

4. Discussion

4.1. Profile data at local scale

Sustainable regional coastal monitoring programs are challenging. It is therefore critical to find a balance between the relevance of collected data and the effort and cost required to maintain the monitoring. In other words, one must define the optimal spatial resolution and data acquisition frequency to get good insight into coastal change and driving factors. Beach-dune systems along the Aquitaine coast, and generally along open coasts, are commonly characterized by high spatial and temporal variability, the relevance of bi-annual profile data is debatable. To further explore the relevance of post-winter profiles combined with the pre-winter LiDAR data to depict long-term morphological seasonal and interannual changes, we used the biweekly beach survey dataset collected at Truc Vert ([Castelle et al., 2020](#)), in the south of the Gironde coast between transects G15.1 and G16. Because Truc Vert topographic data acquired above 6 m NGF are scarce, the volume V_B computed between 2 m and 6 m elevation was used for comparison instead of V_{BD} . [Figure 9](#) shows a comparison of W_B and V_B , highlighting a good agreement with a RMSE of 5.6 m and 26.6 m³/m and a coefficient of determination (r^2) of 0.89 and 0.78, respectively. In particular, the large interannual and seasonal cycles are well reproduced by our dataset, with for instance the strong erosion signature of the 2013-2014 winter in W_B and, to a lesser extent, that of the 2015-2016 winter. This is in line with [Dodet et al. \(2019\)](#) who showed on a number of sandy beaches along the Atlantic coast of Europe that winter-mean wave energy arriving at the coast controls beach interannual variability, while recovery during low-energy periods, on average, has little influence on interannual variability. We anticipate that, combined with other approaches such as satellite imagery (e.g. [Vos et al., 2019](#); [Castelle et al., 2021](#)) and LiDAR data ([Nicolae Lerma et al., 2019](#)), post-winter beach-dune profile surveys adequately distributed along coasts of 10s to 100s kilometres can be relevant to design reliable coastal monitoring programs and provide beach morphology descriptors of interest for coastal managers. Such monitoring program could be replicated along other large-scale sandy barriers at reasonable cost.

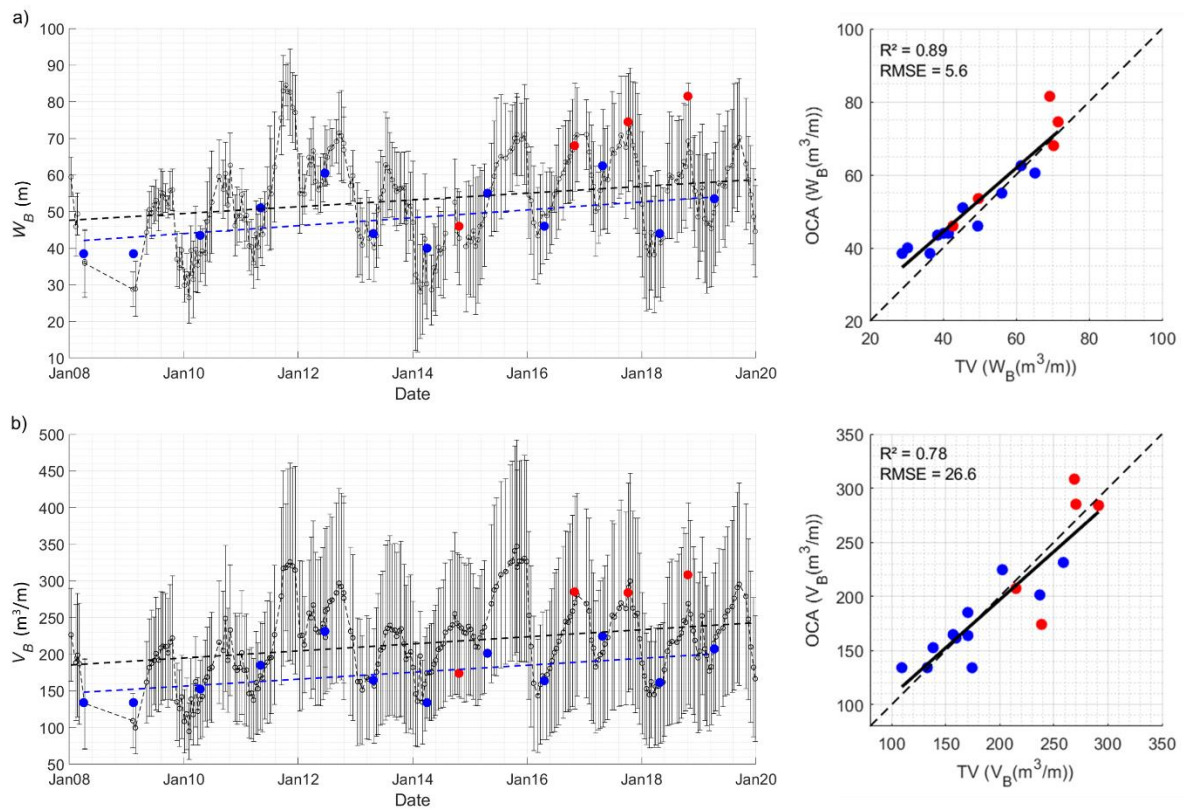


Figure 9: Time series of post-winter (GNSS data in blue) and pre-winter (LiDAR data in red) of (a) beach width W_B and (b) volume V_B computed between 2 m and 6 m NGF, averaged at the two transects surrounding Truc Vert beach (transects G15.1 and G16) compared with Truc Vert biweekly surveys (black dots with vertical error bar indicating alongshore standard deviation at Truc Vert).

4.2. Shoreline change trends

Our study shows that 41 adequately spaced profiles surveyed yearly with GNSS allowed the detailed description of beach-dune response across a 230-km high-energy coast. We also emphasize that including the dune system, even partially, provides more complete insight into coastal erosion and recovery. [Figure 10](#) shows the spatial distribution of x_s position in 2019 with respect to its 2008 position. The most inland and seaward x_s positions during the 2008-2019 period highlight a large spatial variability in shoreline change trajectory. For instance along the Gironde coast at Seg 3.3, x_s varied between +7 and -20 m, eventually coming back near to its 2008 position in 2019. Among the transects

studied, the G18 profile (Seg 4), which is slightly affected by the Arcachon tidal inlet dynamics downdrift, experienced the greatest variability with x_s ranging from +27 to -22 m, but with a near-zero net change over the 2008-2019 period.

Historical orthorectified photograph interpretation has been commonly used to assessment shoreline change on large temporal scale (among many others Dolan et al., 1991; Guillén et al., 1999; Leatherman 2003; Chaaban et al., 2012; Thomas et al., 2014). Figure 10 shows the comparison of our shoreline position change between 2019 and 2008 with the shoreline change rates computed from a diachronic analysis of aerial photographs over the periods 1985-2014 (Bernon et al., 2016) and 1950-2014 (Castelle et al., 2018). Interestingly enough, a very good agreement is observed between these long-term trends and x_s shoreline change observed herein along the entire Gironde coast. In the Landes sector, the dominant erosion trend observed over 1985-2014 in Bernon et al. (2016) is not observed during the last decade, with a large part of the coast being stable or accreting. This is however in line with Castelle et al. (2018) who observed a near-zero long-term trend (not shown) over a different period (1950-2014) in the southern half of the Landes sector.

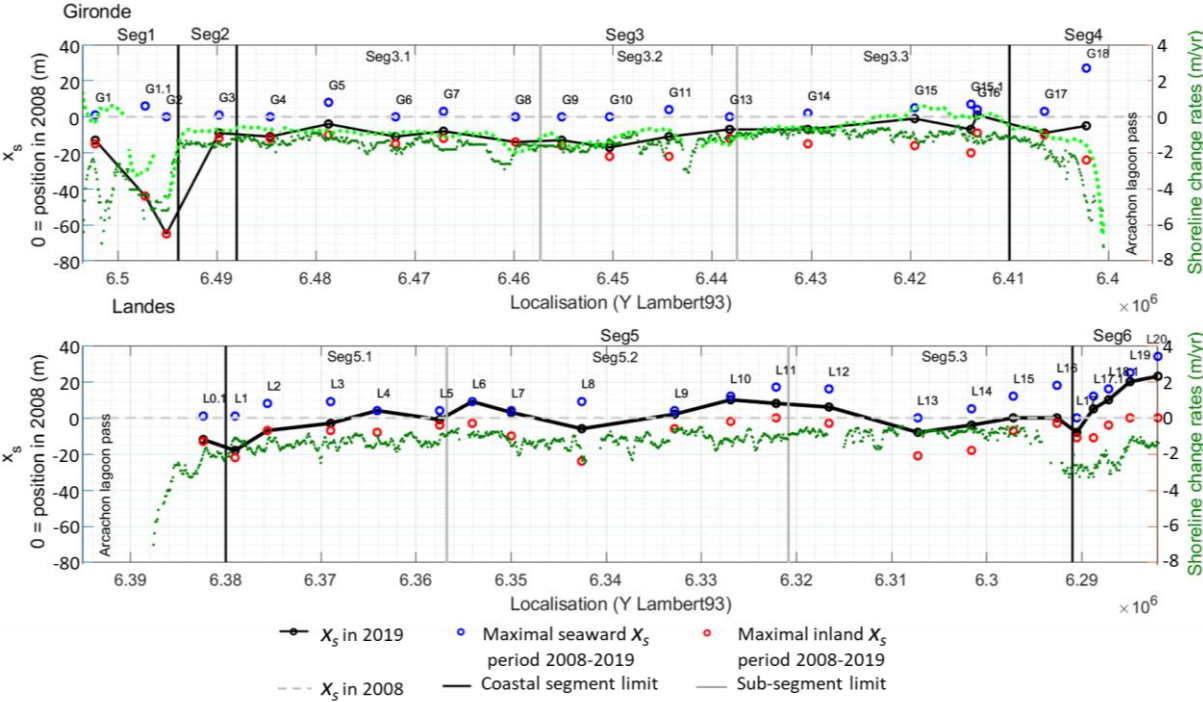


Figure 10: Shoreline position (x_s , circles) with respect to its 2008 position by transect. Shoreline change rates estimated from a diachronic analysis of orthophotos for the periods 1985-2014 (dark green dots) by [Bernon et al. \(2016\)](#), and 1950-2014 (clear green dots) by [Castelle et al. \(2018\)](#).

In areas adjacent to inlets, Gironde estuary (Seg 1), Arcachon inlet (Seg 4) and downdrift of the Capbreton training walls (Seg 6), x_s change patterns contrast with those computed on longer periods in [Bernon et al. \(2016\)](#) and [Castelle et al. \(2018\)](#) from the middle of the 20th century. Shoreline evolution at these segments are responding to more complex processes than the open coast. Morphological changes are affected by inlet dynamics, with variability occurring at sometimes multi-decadal timescales, which deeply affects long-term trends eventually preventing extrapolation of past shoreline evolution trends.

4.3. Regional decadal evolution of the beach-dune system

Our results highlight a strong spatial variability of beach-dune evolution trajectories along the coast ([Figures 11](#)). Schematics of regional variability of beach-dune evolution is shown in [Figure 12](#). Such alongshore variability at the scales of tens of kilometres is commonly attributed to geological factors (e.g. [Jackson et al., 2005](#), [Del Rio et al., 2013](#)), different wave exposure ([Ashton et al., 2001](#)) or artificial shoreline stabilization ([Ells and Murray, 2012](#)). Along the Aquitaine coast, except for the northern and southern extremities of the coast (seg 1 and 6), geological characteristics and forcings (wave and tide) are very similar. However, along the open coast sections a clear latitudinal gradient in beach profile response can be observed ([Figure 12](#)). The stable sectors (in green in [Figure 12](#)) correspond to stretches of coast where gradients in longshore drift are the smallest ([Idier et al., 2013](#)). At the other end of the spectrum, long-term erosion rate along the open coast is maximized where longshore drift diverges, at the limit between Seg 2 and Seg 3 (see [Figures 1 and 5](#)). In between, slow to moderate erosion rates (< 2 m/yr) are observed along sectors where the southerly longshore drift increases southwards.

Although it is well established that seasonal and interannual beach-dune changes in southwest France are primarily driven by cross-shore processes due to changes in incident wave energy (e.g. [Robinet et al., 2016](#)), here we show that gradients in longshore transport are a major control on decadal and multi-decadal shoreline change rate along the open coast. This will need to be further explored using state-of-the-art shoreline changes models (e.g. [Robinet et al., 2020](#)).

In the stable sectors, beach face and dune foot have recovered from the 2013-2014 winter, within 5 years in Gironde (seg 3.3) and within 2 to 3 years in Landes (seg 5.2 and 5.3). Such recovery is smaller in magnitude for the dune face, which is in line with early work showing that recovery is a longer process for the dune than for the beach ([Hesp, 2002](#); [Houser et al., 2015](#)). The sector eroding the most severely, located in the north of the Gironde coast where the longshore drift diverges, shows low and flat dissipative beaches systematically exposing the dune to wave attack during storms. Our results therefore suggest that, except in the vicinity of inlet and estuary mouths, gradients in longshore drift are also the dominant factor explaining sediment availability on the beach and the modes of beach-dune response.

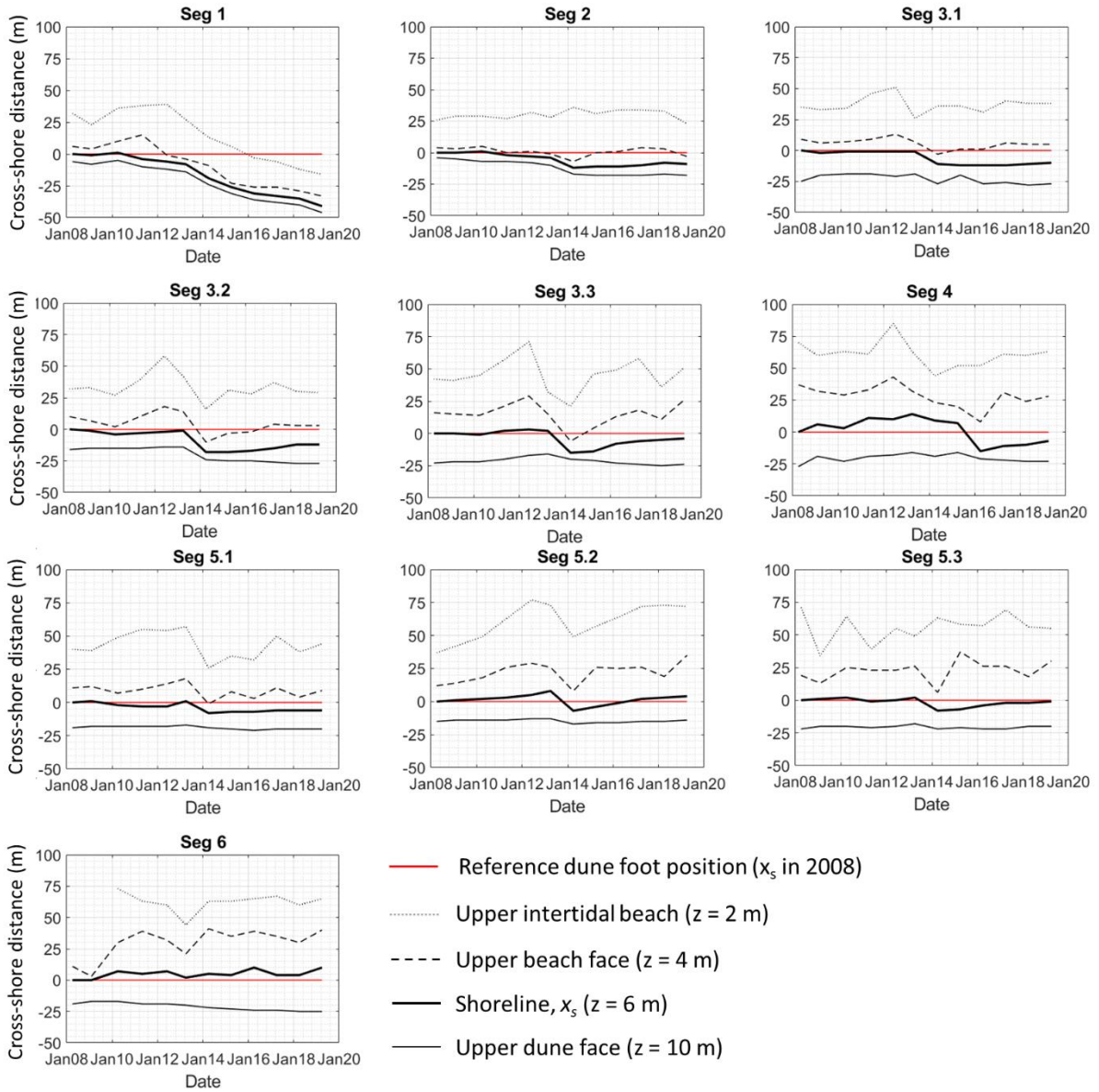


Figure 11: Time series of the segment average cross-shore position of dune face upper limit ($z = 10$ m), shoreline, x_s ($z = 6$ m), upper beach face ($z = 4$ m) and upper limit of the intertidal zone ($z = 2$ m).

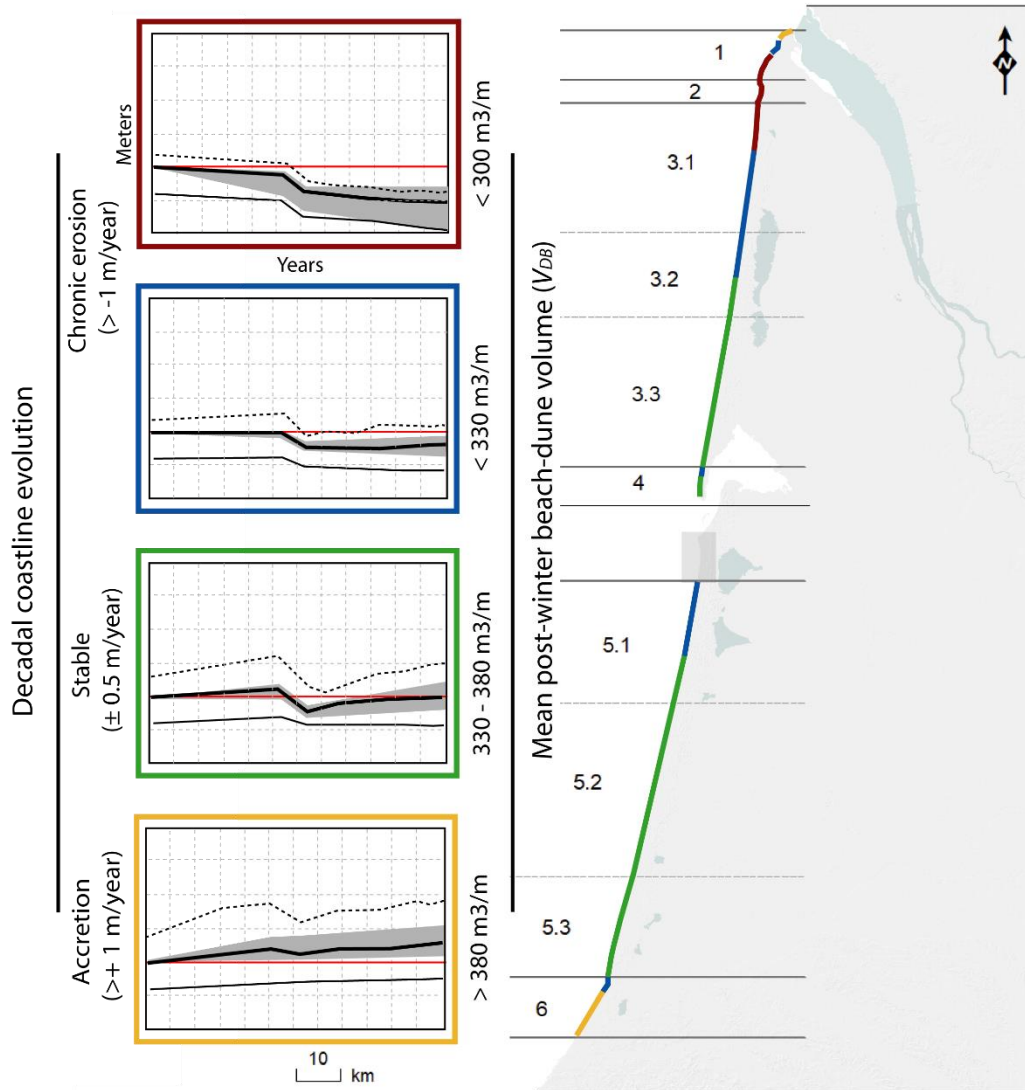


Figure 12: Schematics of regional variability of beach-dune evolution, with in the left-hand panels the reference initial shoreline position x_s (red line). The thick black line shows x_s evolution over the period including a severe winter, the grey area depicts potential alongshore variability), with the upper limit of the dune face (thin black line) and the upper beach position (dashed black line).

5. Conclusion

The 230-km Aquitaine coast is composed of beach-dune systems exposed to high-energy waves, particularly during winter, driving large and alongshore variable morphological changes. A new 11-year

dataset of 41 yearly beach-dune profiles adequately distributed along the coast was used herein, combined with four interspersed LiDAR surveys. Such monitoring strategy allowed addressing the spatial and temporal variability of beach-dune response, including the erosion and subsequent timing and magnitude of recovery from the outstanding 2013-2014 winter. Results show a strong alongshore variability in beach-dune response, with an overall north-south gradient, from chronically eroding dunes backing low dissipative beaches, to slowly accreting dunes backing wide and healthy beaches, through a range of intermediate beach-dune response. The 11-year average shoreline trends are in line with earlier work based on diachronic analysis of georeferenced aerial photographs, with long-term shoreline trends controlled by gradients in longshore transport.

We show that such monitoring program also allows for addressing interannual beach-dune changes, which can be completed with other datasets such as LiDAR surveys. We advocate that after a decade such large-scale coastal monitoring by means of single beach profiles adequately spaced and distributed along 10-100 kilometres of coast is a cheap and efficient approach to address coastal changes at regional scale, to analyse recovery rhythm after extreme events as well as long term trajectories. In addition, in a context of increased erosion and anthropogenic pressure, coastal monitoring programs have become a cornerstone of the development of efficient integrated coastal management strategies in southwest France.

Acknowledgements:

The authors are grateful to the Observatoire de la Côte Aquitaine (OCA) and Brgm for providing data in partnership with the ONF and the IGN (LiDAR). All co-funders of the OCA project are thanked. All Brgm agents who carried out beach profile surveys are also thanked. BC and VM are funded by Agence Nationale de la Recherche (ANR) grant number ANR-17-CE01-0014. This study includes the monitoring study site of Truc Vert labelled by the Service National d'Observation (SNO) Dynalit. The Observatoire de la Côte Aquitaine (OCA) and Observatoire Aquitaine des Sciences de l'Univers (OASU) provide

additional financial support for the Truc Vert beach surveys. ANL, AR, TB, NB and CM thank Brgm for providing support for data analysis and project time for drafting the manuscript

Bibliography

- Anderson, D., Ruggiero, P., Antolínez, J. A. A., Méndez, F. J., Allan, J. (2018). A climate index optimized for longshore sediment transport reveals interannual and multidecadal littoral cell rotations. *Journal of Geophysical Research: Earth Surface*, 123, 1958–1981, doi:10.1029/2018JF004689
- Anthony, E.J. (2013). Storms, shoreface morphodynamics, sand supply, and the accretion and erosion of coastal dune barriers in the southern North Sea. *Geomorphology*, 199, 8-21, doi:10.1016/j.geomorph.2012.06.007.
- Ashton, A. D., A. B. Murray, and O. Arnoult (2001), Formation of coastline features by large-scale instabilities induced by high-angle waves, *Nature*, 414, 296–300.
- Battiau-Queney, Y.; Billet, J.F.; Chaverot, S., and Lanoy-Ratel, P., 2003. Recent shoreline mobility and geomorphologic evolution of macrotidal sandy beaches in the north of France. *Marine Geology*, 194, 31–45.
- Barnard, P. L., Hubbard, D. M., & Dugan, J. E. 2012. Beach response dynamics of a littoral cell using a 17-year single-point time series of sand thickness. *Geomorphology*, 139, 588-598.
- Bernon, N., Mallet, C., & Belon, R. (2016). Caractérisation de l'aléa recul du trait de côte sur le littoral de la côte aquitaine aux horizons 2025 et 2050. Rapport final. BRGM/RP-66277-FR, 99 pp., 48 Ill., 16 tab., 2 ann., 1 CD
- Biausque, M., & Senechal, N. (2019). Seasonal morphological response of an open sandy beach to winter wave conditions: The example of Biscarrosse beach, SW France. *Geomorphology*, 332, 157-169.
- Boak, E.H., Turner, I.L., 2005. Shoreline definition and detection: a review. *J. Coast. Res.* 21 (4), 688-703.

- Bossard, V., & Lerma, A. N. (2020). Geomorphologic characteristics and evolution of managed dunes on the South West Coast of France. *Geomorphology*, 367, 107312.
- Bracs, M. A., Turner, I. L., Splinter, K. D., Short, A. D., & Mortlock, T. R. (2016). Synchronised patterns of erosion and deposition observed at two beaches. *Marine Geology*, 380, 196-204.
- BRGM and ONF (2018). Atlas morphodynamique de la côte sableuse Aquitaine Rapport, BRGM/RP-67152-FR, p. 150p
- Bulteau, T., Nicolae Lerma, A., & Mugica, J. (2016). Caractérisation de l'exposition du littoral Aquitain à l'aléa submersion marine. Rapport final. BRGM/RP-63802-FR.
- Burningham, H. & French, J. (2017) 'Understanding coastal change using shoreline trend analysis supported by cluster based segmentation'. *Geomorphology*, 282 pp. 131-149.
<https://doi.org/10.1016/j.geomorph.2016.12.029>
- Burvingt, O., Masselink, G., Russell, P., & Scott, T. (2017). Classification of beach response to extreme storms. *Geomorphology*, 295, 722-737.
- Castelle, B., Marieu, V., Bujan, S., Splinter, K.D., Robinet, A., Sénéchal, N., Ferreira, S., 2015. Impact of the winter 2013–2014 series of severe Western Europe storms on a double-barred sandy coast: Beach and dune erosion and megacusp embayments. *Geomorphology* 238, 135–148.
<https://doi.org/10.1016/j.geomorph.2015.03.006>
- Castelle, B., Bujan, S., Ferreira, S., Dodet, G., 2017a. Foredune morphological changes and beach recovery from the extreme 2013/2014 winter at a high-energy sandy coast. *Marine Geology*, 385, 41-55.
- Castelle, B., Dodet, G., Masselink, G., Scott, T., 2017b. A new climate index controlling winter wave activity along the Atlantic coast of Europe: The West Europe Pressure Anomaly. *Geophysical Research Letters*, 44, 1384-1392.
- Castelle, B., Guillot, B., Marieu, V., Chaumillon, E., Hanquiez, V., Bujan, S., Poppeschi, C., 2018. Spatial and temporal patterns of shoreline change of a 280-km high-energy disrupted sandy coast from 1950 to 2014: SW France. *Estuarine, Coastal, and Shelf Science*, 200, 212-223.

- Castelle, B., Harley, M.D. (2020). Extreme events: impact and recovery. In: Sandy Beach Morphodynamics, Ed. Jackson, D.W.T. and Short, A.D., 533-556, Elsevier. Castelle, B., Bujan, S., Marieu, V., Ferreira, S. (2020). 16 years of topographic surveys of rip-channelled high-energy meso-macrotidal sandy beach, 7:410, doi:10.1038/s41597-020-00750-5.
- Castelle, B., Masselink, G., Scott, T., Stokes, C., Konstantinou, A., Marieu, V., Bujan, S. (2021). Satellite-derived shoreline detection at a high-energy meso-macrotidal beach. *Geomorphology*, 383, 107707.
- Chaumillon, E., Cange, V., Gaudefroy, J., Mercle, T., Bertin, X., Pignon, C., 2019. Controls on shoreline changes at pluri-annual to secular timescale in mixed-energy rocky and sedimentary estuarine systems. In: Castelle, B. and Chaumillon, E. (eds.), *Coastal Evolution under Climate Change along the Tropical Overseas and Temperate Metropolitan France*. *Journal of Coastal Research*, Special Issue No. 88, pp. 135-156.
- Chaaban, F., Darwishe, H., Battiau-Queney, Y., Louche, B., Masson, E., Khattabi, J. E., & Carlier, E. (2012). Using ArcGIS® Modelbuilder and aerial photographs to measure coastline retreat and advance: North of France. *Journal of Coastal Research*, 28(6), 1567-1579.
- Del Río, L., Gracia, F. J., & Benavente, J. (2013). Shoreline change patterns in sandy coasts. A case study in SW Spain. *Geomorphology*, 196, 252-266.
- Dodet, G., Castelle, B., Masselink, G., Scott, T., Davidson, M., Floc'h, F., Jackson, D.W.T., Suanez, S., 2019. Beach recovery from extreme storm activity during the 2013/14 winter along the Atlantic coast of Europe. *Earth Surface Processes and Landforms*, 44(1), 393-401.
- Dolan, R.; Fenster, M.S., and Holme, S.J., 1991. Temporal analysis of shoreline recession and accretion. *Journal of Coastal Research*, 7, 723–744.
- Ells, K., & Murray, A. B. (2012). Long-term, non-local coastline responses to local shoreline stabilization. *Geophysical Research Letters*, 39(19).

- Guillén, J., Stive, M. J. F., & Capobianco, M. (1999). Shoreline evolution of the Holland coast on a decadal scale. *Earth Surface Processes and Landforms: The Journal of the British Geomorphological Research Group*, 24(6), 517-536.
- Harley, M.D., Turner, I.L., Kinsela, M.A. et al. Extreme coastal erosion enhanced by anomalous extratropical storm wave direction. *Sci Rep* 7, 6033 (2017). <https://doi.org/10.1038/s41598-017-05792-1>.
- Harley, M. D., Turner, I. L., Short, A. D., & Ranasinghe, R. (2011). Assessment and integration of conventional, RTK-GPS and image-derived beach survey methods for daily to decadal coastal monitoring. *Coastal Engineering*, 58(2), 194-205.
- Héquette, A., Ruz, M.H., Zemmour, A., Marin, D., Cartier, A., Sipka, V., 2019. Alongshore Variability in Coastal Dune Erosion and Post-Storm Recovery, Northern Coast of France. In: Castelle, B. and Chaumillon, E. (eds.), *Coastal Evolution under Climate Change along the Tropical Overseas and Temperate Metropolitan France*. *Journal of Coastal Research*, Special Issue No. 88, 25–45.
- Hesp, P. (2002). Foredunes and blowouts: initiation, geomorphology and dynamics. *Geomorphology*, 48(1-3), 245-268.
- Houser, C., Hapke, C., & Hamilton, S. (2008). Controls on coastal dune morphology, shoreline erosion and barrier island response to extreme storms. *Geomorphology*, 100(3-4), 223-240.
- Houser, C., Wernette, P., Rentschlar, E., Jones, H., Hammond, B., & Trimble, S. (2015). Post-storm beach and dune recovery: Implications for barrier island resilience. *Geomorphology*, 234, 54-63.
- Idier, D., Castelle, B., Charles, E., Mallet, C., 2013. Longshore sediment flux hindcast: spatio-temporal variability along the SW Atlantic coast of France. *Journal of Coastal Research* 165, 1785–1790. <https://doi.org/10.2112/SI65-302.1>
- Jackson D.W.T., Cooper J.A.G., Del Río L. (2005). Geological control of beach morphodynamic state, *Marine Geology*, 216 pp. 297-314

- Konlechner, T. M., Kennedy, D. M., O'Grady, J. J., Leach, C., Ranasinghe, R., Carvalho, R. C., & Ierodiaconou, D. (2020). Mapping spatial variability in shoreline change hotspots from satellite data; a case study in southeast Australia. *Estuarine, Coastal and Shelf Science*, 107018.
- Konstantinou, A., Stokes, C., Masselink, G., & Scott, T. (2021). The extreme 2013/14 winter storms: Regional patterns in multi-annual beach recovery. *Geomorphology*, 107828.
- Leatherman, S.P., 2003. Shoreline change mapping and management along the U.S. East Coast. *Journal of Coastal Research*, 38, 5–13.
- Lafon, V., Froidefond, J. M., Lahet, F., & Castaing, P. (2002). SPOT shallow water bathymetry of a moderately turbid tidal inlet based on field measurements. *Remote sensing of Environment*, 81(1), 136-148.
- Larson, M., Kraus, N.C., 1994. Temporal and spatial scales of beach profile change, Duck, North Carolina. *Marine Geology* 117, 75–94.
- Lee, G.H., Nicholls, R.J., Birkemeier, W.A., 1998. Storm-driven variability of the beach-nearshore profile at Duck, North Carolina, USA, 1981–1991. *Mar. Geol.* 148 (3), 163–177.
- Le Mauff, B., Juigner, M., Ba, A., Robin, M., Launeau, P., Fattal, P., 2018. Coastal monitoring solutions of the geomorphological response of beach-dune systems using multi-temporal LiDAR datasets (Vendée coast, France), *Geomorphology*, 304,121-140, doi :10.1016/j.geomorph.2017.12.037.
- Masselink, G., Austin, M., Scott, T., Poate, T., & Russell, P. (2014). Role of wave forcing, storms and NAO in outer bar dynamics on a high-energy, macro-tidal beach. *Geomorphology*, 226, 76-93.
- Morton, R.A., Paine, J.G., Gibeaut, J.C., 1994. Stages and durations of post-storm beach recovery, Southeastern Texas Coast, U.S.A.. *J. Coast. Res.* 10 (4), 884–908.
- Nicolae Lerma A., Bulteau, T., Lecacheux, S., & Idier, D. (2015). Spatial variability of extreme wave height along the Atlantic and channel French coast. *Ocean Engineering*, 97, 175-185.
- Nicolae Lerma, A., Ayache, B., Ulvoas, B., Paris, F., Bernon, N., Bultreau, T., Mallet, C., 2019. Pluriannual beach-dune evolutions at regional scale: Erosion and recovery sequences analysis along the Aquitaine coast based on airborne LiDAR data. *Continental Shelf Research*. 189, 103974.

- Pedreras, R. (2000). Quantification et modélisation du transport éolien au niveau des zones côtières: application au littoral girondin (Doctoral dissertation, Bordeaux 1).
- Phillips, M.S., Blenkinsopp, C.E., Splinter, K.D., Harley, M.D., Turner, I.L., 2019. Modes of berm and beachface recovery following storm reset: observations using a continuously scanning Lidar. *J. Geophys. Res. Earth Surface*, 124.
- Pye, K., & Blott, S. J. (2016). Assessment of beach and dune erosion and accretion using LiDAR: Impact of the stormy 2013–14 winter and longer term trends on the Sefton Coast, UK. *Geomorphology*, 266, 146-167.
- Robinet, A., Castelle, B., Idier, D., Le Cozannet, G., Déqué, M., Charles, E., 2016. Statistical modeling of interannual shoreline change driven by North Atlantic climate variability spanning 2000-2014 in the Bay of Biscay. *Geo-Marine Letters*, 36, 479-490.
- Robinet, A., Idier, D., Castelle, B., & Marieu, V. 2018. A reduced-complexity shoreline change model combining longshore and cross-shore processes: The LX-Shore model. *Environmental modelling & software*, 109, 1-16.
- Robinet, A., Castelle, B., Idier, D., Harley, M.D., Splinter, K.D., 2020. Controls of local geology and cross-shore/longshore processes on embayed beach shoreline variability. *Marine Geology*, 422, doi: 10.1016/j.margeo.2020.106118.
- Ruggiero, P., Voigt, B., & Kaminsky, G. (2000, July). Beach monitoring for enhanced decision-making. In Coastal Society 17th Conference Coasts at the Millennium-Portland, Oregon (pp. 516-524).
- Ruggiero, P., Kaminsky, G.M., Gelfenbaum, G., Voigt, B. 2005. Seasonal to interannual morphodynamics along a high-energy dissipative littoral cell. *J. Coast. Res.*, 213, 553–578.
- Ruiz de Alegria-Arzaburu, A., & Masselink, G. (2010). Storm response and beach rotation on a gravel beach, Slapton Sands, UK *Mar. Geol.* 278, 77–99.
- Sallenger Jr, A. H., Krabill, W. B., Swift, R. N., Brock, J., List, J., Hansen, M., ... & Stockdon, H. (2003). Evaluation of airborne topographic lidar for quantifying beach changes. *Journal of Coastal Research*, 125-133.

- Saye, S. E., Van der Wal, D., Pye, K., & Blott, S. J. (2005). Beach–dune morphological relationships and erosion/accretion: an investigation at five sites in England and Wales using LIDAR data. *Geomorphology*, 72(1-4), 128-155.
- Scott, T., Masselink, G., Russell, P., 2011. Morphodynamic characteristics and classification of beaches in England and Wales, *Marine Geology*, 286, 1-20, doi :10.1016/j.margeo.2011.04.004.
- Scott, T., Masselink, G., O'Hare, T., Saulter, A., Poate, T., Russell, P., Davidson M., Conley D. (2016). The extreme 2013/2014 winter storms: Beach recovery along the southwest coast of England. *Marine Geology*, 382, 224-241.
- SHOM (2016). Références Altimétriques Maritimes, RAM, Edition SHOM p. 120p
- Short, A.D., Wright, L.D., 1983. Physical Variability of Sandy Beaches. In: McLachlan A., Erasmus T. (eds) *Sandy Beaches as Ecosystems. Developments in Hydrobiology*, vol 19. Springer, Dordrecht
- Short, A. D., Bracs, M. A., & Turner, I. L. (2014). Beach oscillation and rotation: local and regional response at three beaches in southeast Australia. *Journal of Coastal Research*, (70), 712-717.
- Stive, M.J.F., 2004. How important is global warming for coastal erosion? An editorial comment. *Clim. Change*, 64, 27-39.
- Stokes, C., Davidson, M. & Russell, P., 2015. Observation and prediction of three-dimensional morphology at a high-energy macrotidal beach. *Geomorphology* 243, 1–13.
- Suanez, S., Cariolet, J. M., Cancouët, R., Ardhuin, F., & Delacourt, C. (2012). Dune recovery after storm erosion on a high-energy beach: Vougot Beach, Brittany (France). *Geomorphology*, 139, 16-33.
- Thomas, T., Lynch, S. K., Phillips, M. R., & Williams, A. T. (2014). Long-term evolution of a sand spit, physical forcing and links to coastal flooding. *Applied Geography*, 53, 187-201.
- Turner, I.L., Harley, M.D., Short, A.D., Simmons, J.A., Bracs, M.A., Phillips, M.S., Splinter, K.D., 2016. A multi-decade dataset of monthly beach profiles and inshore wave forcing at Narrabeen, Australia. *Scientific Data*, 2, 160024.
- Tucker M.J. and Pitt E.G. (2001) *Waves in ocean engineering*. Elsevier, Oxford

Vos, K., Harley, M.D., Splinter, K.D., Simmons, J.A., Turner, I.L., 2019. Sub-annual to multi-decadal shoreline variability from publicly available satellite imagery, Coastal Engineering, doi:10.1016/j.coastaleng.2019.04.004.